EASR

Engineering and Applied Science Research

https://www.tci-thaijo.org/index.php/easr/index

Published by the Faculty of Engineering, Khon Kaen University, Thailand

Conversion of methyl methacrylate to methyl isobutyrate via hydrogenation over Ni/zeolites catalysts

Ramzi Saif[1)], Surachet Hongkailers[1)] and Napida Hinchiranan*[1, 2, 3)]

[1)]Department of Chemical Technology, Faculty of Science, Chulalongkorn University, Bangkok 10330, Thailand
[2)]Center of Excellence on Petrochemical and Materials Technology (PETROMAT), Chulalongkorn University, Bangkok 10330, Thailand
[3)]Center of Excellence in Catalysis for Bioenergy and Renewable Chemicals (CBRC), Chulalongkorn University, Bangkok 10330, Thailand

Received 8 September 2023
Revised 22 November 2023
Accepted 8 December 2023

Abstract

According to the zero waste and upcycling policy, this work aims to utilize waste polymethyl methacrylate (PMMA) by its conversion to methyl isobutyrate (MIB) via hydrogenation over nickel (Ni) based catalysts supported on the commercial zeolites: HY, H-Beta-27 (SiO_2/Al_2O_3 mol ratio = 27), H-Beta-40 (SiO_2/Al_2O_3 mol ratio = 40), and H-ZSM-5. The appropriate catalyst support was first screened by using MMA monomer as the substrate for hydrogenation. Under 30 bar initial hydrogen pressure (P_{H2}) at 250 °C for 3 h, the Ni/H-beta-27 catalyst effectively promoted hydrogenation to achieve an 85% MMA conversion level with a 56.2 wt% MIB yield because of its larger external surface area and pore size. A higher initial P_{H2} (40 bar) and longer reaction time (5 h) improved the MIB yield up to 84.6 wt%. For hydrogenation of the MMA portion in a pyrolysis liquid product derived from waste PMMA, a MMA conversion level of 99.7% was achieved when hydrogenation was operated under 30 bar initial P_{H2} and 250 °C for 5 h. However, only a 36.3 wt% MIB yield was obtained with a noticeable formation of coupling and cyclic compounds at 42 wt% and 18 wt%, respectively. The enhancement of the initial P_{H2} to 40 bar overcame this problem and increased the MIB yield to 47.6 wt%.

Keywords: Hydrogenation, Methyl isobutyrate, Methyl methacrylate, Catalyst

1. Introduction

Polymethyl methacrylate (PMMA) is a transparent thermoplastic with unique properties, such as a high optical clarity, safer than glass, and a low density, making it suitable for use in various applications, including aircraft windows, automobile parts, electronics, protective coating, and artificial marble, etc. [1]. However, only 30,000 tons of spent PMMA are currently collected and recycled in Europe, compared to a global production capacity of 2.4 x 10^6 tons. This highlights the opportunities in the field of PMMA recycling, taking into account the fact that the energy required for the synthesis of virgin MMA is relatively high [2].

Pyrolysis (thermal cracking) is one of the appropriate methods to convert the spent or waste PMMA to chemicals or feedstock recycling. This process is well-known and regarded as the most effective way to obtain a high-quality product. Pyrolysis also depolymerizes the waste PMMA to recover MMA monomer [3]. Accordingly, the expansion of MMA usage should be considered due to the increased MMA production capacity and PMMA surplus. One appropriate way is to use MMA as a feedstock for producing methyl isobutyrate (MIB), which is an intermediate in the production of isobutyric acid (IB), a precursor to produce valuable commodity chemicals [4]. For example, IB is needed to synthesize 2,2,4,4-tetramethyl-1,3-cyclobutanediol, a commercialized co-polyester to produce clear and bisphenol A-free plastics [5]. Moreover, the application of IB is involved in the manufacture of many products, such as resins, beverage additives, coatings, adhesive agents, inks, paints, plasticizers, etc. [6]. Currently, IB is generated by the Koch carbonylation of propene catalyzed by acid [7]. However, two significant drawbacks are induced in this process – (i) the use of non-renewable fossil fuels to obtain propene and (ii) its high energy requirement. Moreover, this process uses harmful chemicals, such as sulfuric acid, hydrogen fluoride, and boron fluoride [6].

Regarding the trend of recycling/upcycling to utilize waste plastics, MIB can be directly produced by hydrogenation of MMA recovered from the thermal cracking of waste PMMA. The obtained MIB can then be further processed to obtain IB via hydrolysis process in a separate step [8]. At present, the catalysts reported for the hydrogenation of MMA are all precious noble metal catalysts. Zhou et al. [8] studied the hydrogenation of MMA over ruthenium (Ru) catalyst supported on activated carbon obtained from bio-reduction, including the effect of the applied reaction conditions on the efficiency of the catalyst. The experimental results demonstrated that 100% MMA conversion was achieved when the system was operated under a pressure of 40–60 bar. Aldea and Alper [9] reported that montmorillonite supported Ru-clays could catalyze the hydrogenation of MMA with a MMA conversion level and MIB yield of 100% and 85–91%, respectively, at 75 °C under 40 bar hydrogen (H_2) pressure (P_{H2}) for a long reaction time (45 h). Kim and Kim [10] investigated the hydrogenation of olefins over palladium (Pd) supported on magnetic nanoparticles. In the case of MMA hydrogenation,

*Corresponding author.
Email address: napida.h@chula.ac.th
doi: 10.14456/easr.2024.15

the yield of MIB in the presence of methanol was 97% at room temperature under 1 atm P_{H2}. However, complicated separation and purification processes were required to eliminate the methanol from the obtained product. Similarly, Natour and Abu-Reziq [11] applied a Pd-based catalyst supported on a magnetically separable polyurea to selectively hydrogenate α,β-unsaturated compounds, and achieved 100% MMA conversion within 2 h at 50 °C.

Among the non-noble active metals used in the selective hydrogenation, such as iron (Fe), cobalt (Co), nickel (Ni), and copper (Cu) [12, 13], Ni-based catalysts are normally applied to the hydrogenation of olefins or unsaturated compounds due to their availability and cost effectiveness compared to the precious noble metals like platinum (Pt) or Pd (Ni is about 1000 times cheaper than Pt [14]). These Ni-based catalysts have a high performance in the hydrogenation of various unsaturated substrates, such as phenylacetylene to styrene [15], fatty acid methyl esters derived from palm oil [16], and aromatic compounds [17].

With respect to the catalyst supports, the acidic zeolite supports exhibit a positive impact on the hydrogenation activity of Ni-based catalysts. Song et al. [18] revealed that the acidic sites of the zeolites in the vicinity of the Ni metal induced a high rate of hydrogenation and hydrogenolysis. In the present article, the active Ni metal supported on various zeolites was evaluated in the conversion of MMA to MIB via hydrogenation. This article consists of two parts. The first part involves the use of analytical grade MMA monomer to screen for the appropriate zeolite support and to then evaluate the influence of various reaction parameters (reaction temperature, initial P_{H2}, and reaction time) on the MMA hydrogenation and the yields of the obtained products (MIB, IB, and coupling compounds). The appropriate zeolite was selected as the support for Ni catalyst based on these results and then was used in the second part for the hydrogenation of the MMA portion in the pyrolysis liquid product derived from waste PMMA (PL-WPMMA) without any purification under the given reaction conditions. Moreover, the reusability of the catalyst was reported.

2. Materials and methods

2.1 Materials and chemicals

The waste PMMA used in this research was the spent rotors used in veterinary diagnosis (VETSCAN VS2, Zeotis). The MMA monomer (AR grade, 99% purity) and analytical grade nickel (II) nitrate hexahydrate [$Ni(NO_3)_2{\cdot}6H_2O$] were purchased from Sigma-Aldrich (Singapore). The commercial grade zeolites obtained from TOSOH Co., Ltd. (Japan): HY (331HSA; SiO_2/Al_2O_3 mol ratio = 3), NH_4-ZSM-5 (820NHA; SiO_2/Al_2O_3 mol ratio = 20), H-Beta (940HOA; SiO_2/Al_2O_3 mol ratio = 40), and NH_4-beta (930NHA; SiO_2/Al_2O_3 mol ratio = 27) were used as received. The H_2 (≥ 99.99%), nitrogen (N_2; ≥ 99.99%), and 5% (v/v) oxygen (O_2)/N_2 were supplied from Thai - Japan Gas Co., Ltd. (Thailand). Acetone (≥ 99.95%, RCI Labscan, New Zealand) was applied as the solvent for sample preparation in gas chromatography-mass spectrometry (GC-MS) analysis.

2.2 Catalyst preparation

All zeolites were first calcined in air at 550 ◦C at a heating rate of 10 ◦C/min for 5 h to transform the zeolites from the NH_4-form to the H-form and eliminate some impurities on the zeolite's surface. Incipient wetness impregnation was then applied to prepare the monometallic Ni catalysts from $Ni(NO_3)_2{\cdot}6H_2O$. This Ni precursor (9.91 g) was dissolved in the deionized water to obtain a 1.7 M $Ni(NO_3)_2{\cdot}6H_2O$ solution and then impregnated onto the calcined zeolites (20 g). After evaporating the excess water at 65 °C for 30 min in a rotary evaporator, the resulting catalyst was dried at 110 °C for 12 h and calcined in air at 500 °C (heating rate = 10 °C/min) for 4 h to give 10 wt% NiO/zeolite catalysts. The calcined catalysts were then reduced in a quartz tube placed in a horizontal furnace in the presence of a H_2 stream at a flow rate of 20 mL/min and 500 °C for 2 h followed by passivation in a stream of 5% (v/v) O_2/N_2 gas mixture at a flow rate of 2 mL/min and room temperature overnight. The name of the obtained catalysts was assigned as Ni/H-ZSM-5, Ni/HY, Ni/H-beta-27, and Ni/H-beta-40, where 27 and 40 were the mole ratio of SiO_2/Al_2O_3 of each beta zeolite.

2.3 Characterization of catalysts

The specific surface area, pore volume, and pore size of the passivated Ni-based catalysts were evaluated from the N_2 adsorption–desorption isotherms recorded at −196 °C using an area and porosity analyzer (3P Instruments, 3P micro300). After placing the passivated catalyst (ca. 60 – 80 mg) in a sample holder, the system was operated under vacuum with a final temperature of the outgas at 300 °C for 3 h. The Brunauer-Emmett-teller (BET) equation and t-plot method were applied to calculate the specific surface area of the catalyst samples (S_{BET}) and the micropore surface areas (S_{micro}), respectively. The external surface area (S_{ext}) was evaluated from the difference between S_{BET} and S_{micro} [19]. The total pore volume (V_{total}) and the average pore diameter (D_{ave}) were also reported.

Type and crystalline matters (metallic Ni and NiO) in each catalyst were obtained using X-ray diffractometry (XRD; Bruker D8 advance) with Cu-Kα radiation (40 kV, 40 mA, and λ = 0.15406 nm). The 2θ was scanned in the range of 35–80° at a rate of 1°/s. The size of the metal particles was measured and calculated using the Scherer equation [20].

Ammonia-temperature-programmed desorption (NH_3-TPD; BELCAT II Belcat-Basic chemisorption analyzer) was used to determine the acidity of the passivated catalysts. After pretreating the catalyst samples at 300 °C in the presence of helium (He) at a flow rate of 50 mL/min for 30 min, the NH_3 adsorption step was induced under 5% (v/v) NH_3/He gas stream at a flow rate of 50 mL/min for 30 min. The system was then flushed with He gas (flow rate = 50 mL/min) at 100 °C for 30 min to remove the adsorbed and non-adsorbed NH_3. Subsequently, the sample was heated under a He atmosphere (flow rate = 30 mL/min) from 100 °C to 800 °C at 10 °C/min and a thermal conductivity detector (TCD) was used to detect the amount of desorbed NH_3.

The reduction temperature of each catalyst was determined using the H_2-temperature-programmed reduction (H_2-TPR) mode in a Belcat-Basic chemisorption analyzer (BELCAT II). The samples were first pretreated under argon (Ar) gas (flow rate = 50 mL/min) at 110 °C for 30 min. The pretreated catalysts were then reduced under a 5% (v/v) H_2/Ar mixed gas at a flow rate of 30 mL/min as the temperature of the sample cell was progressively increased from 100 °C to 900 °C at 10 °C/min.

2.4 Preparation of PL-WPMMA

After crushing into small pieces, the spent PMMA rotor (30 g) was pyrolyzed in a fixed bed reactor at 400 °C at a heating rate of 5 °C/min under N_2 gas at a flow rate of 100 cm^3/min and held at 400 °C for 30 min. The pyrolysis vapor was trapped in glass tubes immersed in an ice bath. This condition provided a 95.5 wt% PL-WPMMA yield containing 78 wt% MMA.

2.5 Hydrogenation of MMA and PL-WPMMA

The MMA monomer or PL-WPMMA (4 g) was transferred into a 20-mL high pressure batch reactor containing a magnetic stirrer bar and the passivated catalyst (0.4 g). Before starting the reaction, the air inside the reactor was removed by flushing with H_2 gas for 15 min. Subsequentially, H_2 was charged into the reactor at the desired P_{H2} and then heated to the target reaction temperature before starting the stirrer, which was kept constant at 700 rpm. After holding for the given reaction time interval, the reactor was immersed in water to cool the system to room temperature to stop the reaction. The spent catalyst separation involved a two-step process. First, the spent catalyst was separated from the liquid product using centrifugation at 10,000 rpm for 10 min to ensure the effective removal of the catalyst from the liquid phase. Subsequently, the separated spent catalyst was washed with acetone before drying at 110 °C for 12 h for reuse.

2.6 Product analysis

The chemical compositions in the liquid product obtained from hydrogenation consisted of MIB, IB, and coupling compounds. They were distinguished by gas chromatography-mass spectrometry (GC-MS; Shimazu-2876) coupled with a DB-5MS column (0.25 mm inner diameter; 30 m length) and using He as the carrier gas at a flow rate of 1.0 mL/min. The liquid product was diluted in acetone to 1,000 ppm before analysis. The column temperature was initially set at 40 °C for 2 min and then raised to 200 °C at 5 °C /min, and finally elevated to 280 °C at 15 °C /min and held at this temperature for 5 min.

The MMA conversion was analyzed using GC coupled with a flame ionization detector (GC-FID; Agilent 7890A) and a HP-5 column, with the MMA levels being calculated by reference to calibration curves. The GC oven temperature was increased from 50 °C to 250 °C at 10 °C /min and held at 250 °C for 2 min using He as the carrier gas at a flow rate of 2.4 mL/min. The detector's temperature was set at 300 °C using an air/H_2 flame. The selectivity of each composition in the liquid product was analyzed from the peak area obtained from the GC-MS chromatogram. The MMA conversion level and the yield of chemical compositions were defined as shown in Eqs. (1) and (2), respectively. The i^{th} selectivity of each component was obtained from its relative peak area in the GC-MS chromatograms.

$$\text{MMA conversion (\%)} = \left[1 - \frac{\text{Unreacted MMA content (mole)}}{\text{Initial MMA content (mole)}}\right] \times 100 \quad (1)$$

$$i^{th}\text{ product yield (\%)} = \frac{i^{th}\text{ selectivity} \times \text{MMA conversion}}{100} \quad (2)$$

3. Results and discussion

3.1 Characterization of catalysts

The surface area, pore volume and pore size of the prepared catalysts were evaluated from N_2 adsorption-desorption isotherms (Figure 1a) and are summarized in Table 1. The Ni/H-ZSM-5 and Ni/HY showed a type I isotherm. However, the N_2 adsorption-desorption isotherms of Ni/H-Beta-40 and Ni/H-Beta-27 were a combination of types I and IV following the IUPAC classification. The hysteresis loop in the Ni/H-Beta-40 and Ni/H-Beta-27 catalysts was classified as the H4 type, suggesting that they had a mesoporous structure [21, 22], whereas Ni/H-ZSM-5 and Ni/HY did not show a hysteresis loop, but they exhibited microporous characteristics. However, the Ni/H-Beta-27 catalyst demonstrated a continuous N_2 adsorption to reach a maximum adsorbed quantity of 274 cm^3/g at a high relative pressure due to its high S_{ext} (238 m^2/g; Table 1). This phenomenon was generated from the aggregation of small crystallites to form interparticle mesopores during Beta zeolite preparation [23]. The mesopores of the Ni/H-Beta-27 catalyst also provided the largest V_{total} (0.41 cm^3 /g) and D_{ave} (3.31 nm), as shown in Figure 1b and Table 1.

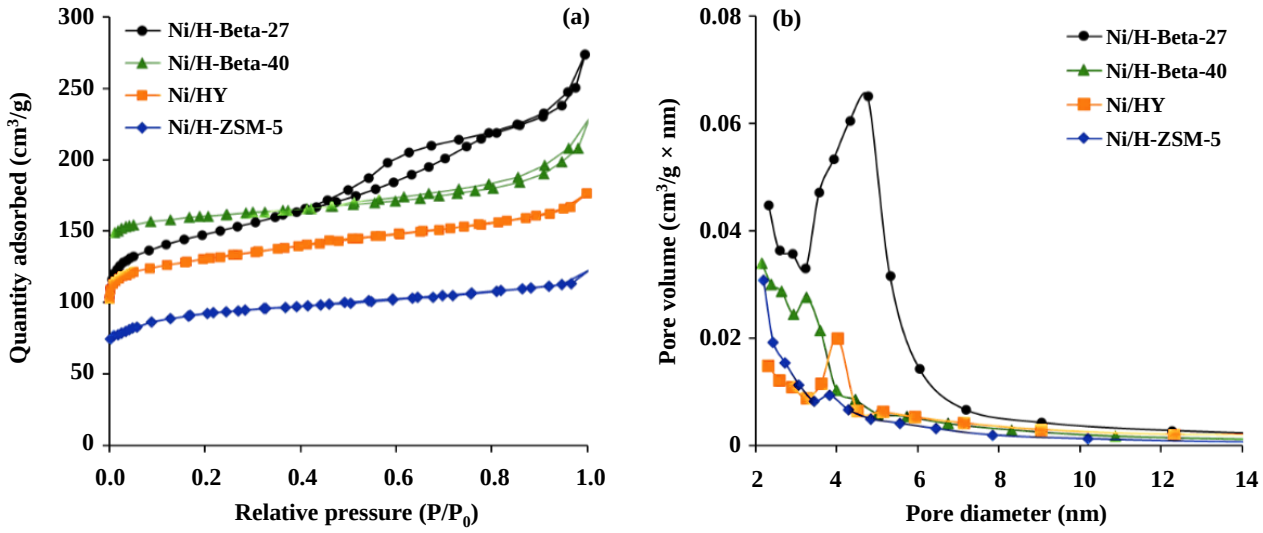

Figure 1 Textural properties of the passivated Ni-based catalysts. Representative (a) N_2 adsorption-desorption isotherms and (b) BJH pore size distribution in the adsorption mode.

Table 1 Textural properties, particle size, H_2 consumption during reduction, and total acidity of the Ni-based catalysts

Catalyst	Specific area (m^2/g)			V_{total}[4] (cm^3/g)	D_{ave}[5] (nm)	Particle size (nm)[6]		H_2 consumption (mmol/g)[7]	Total acidity (μmol NH_3/g)
	S_{BET}[1]	S_{micro}[2]	S_{ext}[3]			NiO	Ni		
Ni/H-ZSM-5	305	226	79	0.18	2.42	16.8	24.5 (45.8%)[8]	0.97	1,048
Ni/HY	526	449	77	0.33	2.54	18.7	21.5 (15.0%)	0.69	1,638
Ni/H-Beta-40	439	303	136	0.27	2.45	14.0	19.1 (36.4%)	0.88	897
Ni/H-Beta-27	502	264	238	0.41	3.31	14.0	14.3 (2.14%)	0.84	1,157

[1]S_{BET} = BET surface area; [2]S_{micro} was determined by t-method analysis; [3]S_{ext} was calculated from the difference between S_{BET} and S_{micro}; [4] V_{total} = total pore volume; [5]D_{ave} = average pore diameter; [6]Estimated from Scherrer Equation by using the peaks at 2θ of 37.2° and 44.4° for NiO and Ni phase in the XRD pattern, respectively; [7]Obtained from H_2-TPR analysis; [8] Percentage change of the metal particle size after reduction and passivation.

The XRD patterns of the calcined and passivated catalysts are shown in Figure 2. For the calcined catalysts, Figure 2a showed that the reflection signals of the NiO phase of all catalysts appeared at 2θ of 37.2°, 43.3°, 62.9°, and 75.3° [24]. After reduction and passivation (Figure 2b), the Ni/H-ZSM-5 and Ni/HY catalysts had new peaks with a high intensity at 44.4° and 51.8°, which were attributed to the Ni phase [25], while the peaks of NiO had almost disappeared. However, the opposite results were observed for the passivated Ni/H-Beta-40 and Ni/H-Beta-27 catalysts, where the small peaks of the NiO phase were clearly observed. Moreover, their reflection signals were broader with a lower intensity, which implied that the Ni/H-Beta-40 and Ni/H-Beta-27 catalysts had a stronger metal-support interaction. Moreover, the NiO particle size of Ni/H-beta-40 and Ni/H-beta-27 was smaller than those of the Ni/H-ZSM-5 and Ni/HY catalysts (Table 1). It was possible that the lower level of agglomeration of NiO with its higher dispersion could uniformly cover the surface of H-Beta-40 and H-Beta-27 resulting in the broader and lower peak intensity in the XRD patterns. This was possibly due to the effect of the higher S_{ext} to promote a more even metal dispersion [22]. After reduction and passivation, the size of the NiO particles in all catalysts was smaller than that of the Ni particles (Table 1), suggesting that the high reduction temperatures induced agglomeration of Ni particles (see the following H_2-TPR section for further explanation of the significant variation observed in the Ni crystallite size).

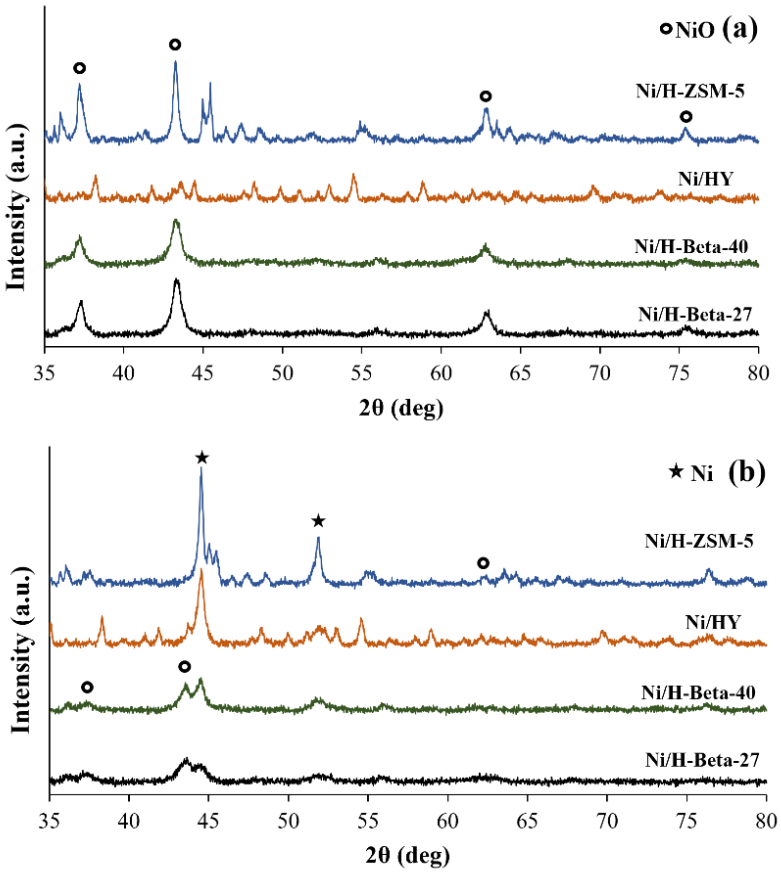

Figure 2 Representative XRD pattern of Ni-based catalysts: (a) calcined and (b) passivated forms.

The reducibility, as measured from the amount of H_2 consumption, and reduction temperature of each catalyst was evaluated by H_2-TPR (Figure 3). The various reduction temperatures of NiO involve the different positions in the framework of zeolite interacting with the cationic Ni species [26]. For all catalysts, two superimposed reduction peaks demonstrated the simultaneous existence of easily and hardly reduced Ni^{2+} species on the zeolite's surface. The first peak appeared at below 500 °C (α-peak), which corresponded to the reduction of the NiO particles deposited on the outer zeolite's surface [27]. Whereas, the second peak was observed at reduction

temperatures higher than 500 °C (β-peak) and corresponds to the reduction of NiO particles deposited inside the zeolite's cavities, including the channels and cages of the zeolite's structure [27], and reflects the higher diffusional restrictions during the reduction [28]. The intensity of the α-peak in Ni/H-Beta-40 and Ni/H-ZMS-5 catalysts was much higher than those of Ni/H-Beta-27 and Ni/HY, suggesting that NiO particles on the Ni/H-Beta-40 and Ni/H-ZSM-5 catalysts were partially deposited at the outer surface of zeolite. Thus, the complete reduction of the NiO α-peak at a high reduction temperature led to an agglomeration of Ni species on the Ni/H-Beta-40 and Ni/H-ZSM-5 catalysts resulting in the larger Ni particle size compared to the Ni/H-Beta-27 and Ni/HY catalysts (Table 1). Considering the same zeolite structure, the Ni/H-Beta-40 showed a higher α-peak intensity, while the Ni/H-Beta-27 exhibited a greater reduction of the β-peak, which might be related to their difference in acidity and aluminum content [28].

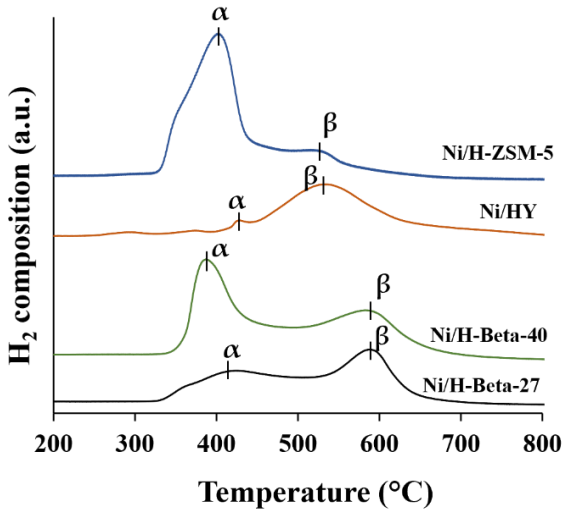

Figure 3 Representative H_2-TPR profiles of the calcined Ni/zeolite catalysts.

The total acidity of the catalysts was also evaluated by NH_3-TPD technique (Figure 4 and Table 1). The acidity of the zeolite supports typically corresponded to the SiO_2/Al_2O_3 ratio of the zeolite framework, where the higher SiO_2/Al_2O_3 ratio indicated the lower concentration of acidic sites. The Ni/HY catalyst had the greatest total acidity of 1,638 μmol NH_3/g due to the lowest SiO_2/Al_2O_3 ratio of 3, while the Ni/H-Beta-40 catalyst with a SiO_2/Al_2O_3 ratio of 40 showed the lowest total acidity of 897 μmol NH_3/g (Table 1).

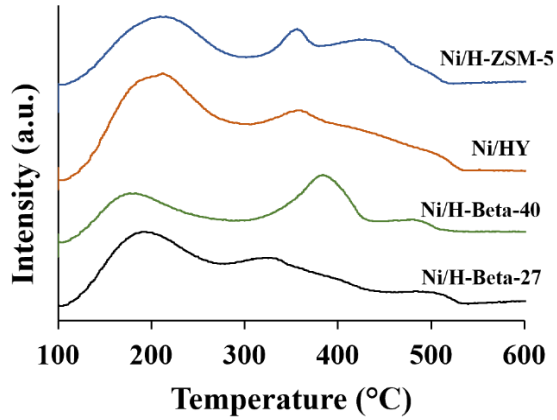

Figure 4 Representative NH_3-TPD profiles of the passivated Ni/zeolite catalysts.

3.2 Hydrogenation of MMA monomer

To maximize the MIB yield obtained from hydrogenation of the MMA monomer, the distribution of liquid, solid, and gaseous products from the MMA hydrogenation was investigated whilst varying the reaction parameters of the zeolite types, reaction time, reaction temperature, and initial P_{H2} (see Table 2). For the effect of the zeolite type, the MMA hydrogenation was operated under 30 bar initial P_{H2} at 250 °C for 3 h. The system operated in the absence of catalyst was also investigated for comparison. Without the catalyst, a liquid product yield of 94.1 wt% with a small amount of gas formation (5.9 wt%) was obtained, possibly due to the thermal cracking induced during the 250 °C reaction for 3 h. However, no solid product was observed. When the Ni-based catalysts with different acidities were applied to hydrogenate the MMA monomer, the yields of liquid and gas products were markedly decreased to 79.1–81.0 wt% and 4.3–5.0 wt%, respectively, with a corresponding formation of 14.4–16.6 wt% solid residue (Table 2; Entries 2–5). This result reflects the role of the acidity of each catalyst [22, 29]. The system using the Ni/H-ZSM-5 catalyst with the highest acidity (1,638 μmol NH_3/g) generated the largest amount of solid product (16.6 wt%). This phenomenon was also affected by the catalyst's smallest pore size of 2.42 nm, as the large organic compounds generated during hydrogenation could be trapped and then form the solid residues in the cages of the acidic zeolite-supports [30].

Table 2 Effect of the zeolite type and reaction conditions on the product distribution obtained from the hydrogenation of analytical grade MMA monomer

Entry	Catalyst	Temperature (◦C)	Initial P_{H2} (bar)	Time (h)	Product yield (wt%)		
					Liquid	Solid	Gas
1	Without catalyst	250	30	3	94.1	0.00	5.90
2	Ni/H-ZSM-5	250	30	3	79.1	16.6	4.25
3	Ni/HY	250	30	3	80.1	15.1	4.75
4	Ni/H-Beta-40	250	30	3	81.0	14.7	4.25
5	Ni/H-Beta-27	250	30	3	80.6	14.4	5.00
6	Ni/H-Beta-27	250	30	5	84.7	10.6	4.70
7	Ni/H-Beta-27	250	30	7	88.8	4.43	6.75
8	Ni/H-Beta-27	250	30	9	88.9	2.82	8.25
9	Ni/H-Beta-27	250	10	5	77.0	19.2	3.75
10	Ni/H-Beta-27	250	20	5	80.1	15.4	4.50
11	Ni/H-Beta-27	250	40	5	94.7	0.54	4.75
12	Ni/H-Beta-27	230	30	5	80.7	15.3	4.00
13	Ni/H-Beta-27	270	30	5	88.9	5.32	5.75
14	Ni/H-Beta-27	290	30	5	93.9	0.12	6.00

The chemical composition of the liquid products obtained from the MMA hydrogenation using the Ni/H-Beta-27 catalyst were examined using GC-MS analysis (Figure 5) are shown as representatives. At a reaction condition of 30 bar initial P_{H2} and 250 °C for 3 h, the obtained liquid product contained 56.7 wt% MIB with small amounts of IB and coupling compounds (dimethyl 2,5-dimethylhex-2-enedioate and dimethyl 2-methyl-5-methylenehexanedioate).

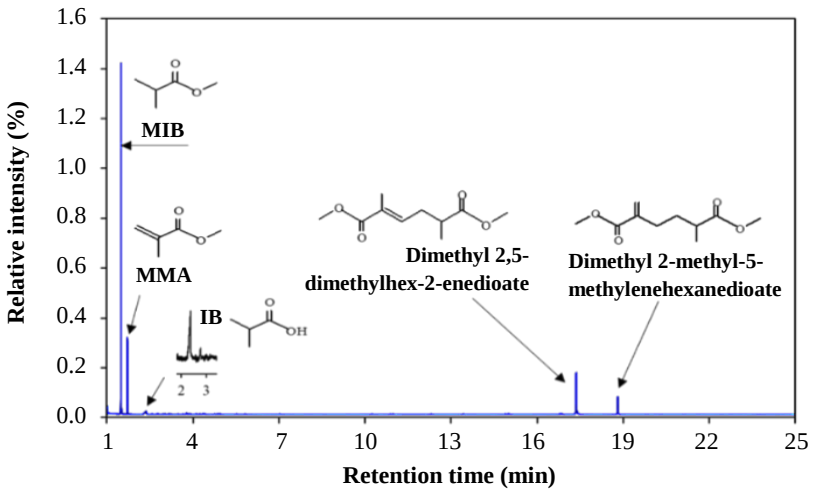

Figure 5 Representative GC–MS chromatogram of the liquid product produced from hydrogenation of MMA monomer over the Ni/H-Beta-27 catalyst at 30 bar initial P_{H2} and 250 °C for 3 h.

The influences of the reaction parameters, such as zeolite type, reaction time, initial P_{H2}, and reaction temperature on the MMA conversion level and the yields of MIB, IB, and coupling compounds are summarized in Figure 6. In the absence of the Ni-based catalyst, the MMA conversion level was 65.5% when the system was operated under 30 bar initial P_{H2} for 3 h (Figure 6a). However, the MIB yield in the obtained liquid product was less than 4 wt% with coupling compounds being promoted as the dominant products (ca. 40 wt%). Although the reaction was performed under H_2 atmosphere, the results exhibited that the hydrogenation of MMA to MIB could not be activated unless the appropriate catalysts were applied.

The activity of the catalyst did not only depend on the active metal, but it was also affected by the support used to prepare the catalysts. Here, this part aimed to evaluate the appropriate zeolite support for the Ni-based catalyst in MMA hydrogenation (operated under the same condition as used for the non-catalytic process).

The Ni catalysts supported on H-Beta-27, H-Beta-40, and HY provided ca. 83% MMA conversion level, while the system using Ni/H-ZSM-5 catalyst had a lower MMA conversion level of 78% (Figure 6a). This was due to the Ni/H-ZSM-5 catalyst's low S_{BET} and V_{total}. Moreover, the support geometry also influences product selectivity. The Ni/H-Beta-27 catalyst provided the highest MIB yield (56.2 wt%) was due to its largest D_{ave} and S_{ext} that provided the higher molecular diffusion of MMA into the catalyst's pores. Moreover, the high reactivity of the passivated Ni/H-Beta-27 catalyst for MMA hydrogenation (Figure 2b) possibly involved the existence of NiO phase. Previous works have reported a synergistic effect of Ni-NiO to effectively promote the hydrogenation of furfural to cyclopentanone [31] and levulinic acid to γ-valerolactone [32]. Indeed, the combination of Ni and NiO phases in the catalyst exhibited and 18- and 10-times higher activity for levulinic acid hydrogenation than NiO and metallic Ni, respectively [32]. Although

NiO was not active for hydrogenation, NiO could provide the strong adsorption of certain substrates due to its polar surface [33]. For metallic Ni, H_2 could be adsorbed on the Ni surface followed by H_2 dissociation to produce the active hydrogen atom [32]. With the combination of Ni and NiO phases in the catalysts, the adsorbed substances on the NiO phase could react with the adsorbed H on the adjacent metallic Ni to provide the desired saturated compounds following the Langmuir-Hinshelwood mechanism [32].

With respect to the Ni/HY and Ni/H-ZSM-5 catalysts, they exhibited a lower conversion of MMA to MIB, which was possibly due to the influence of their higher acidity that enhanced the probability of dimerization of MMA [34, 35]. Their XRD pattern (Figure 2b) also indicated the almost complete reduction of the NiO phase in the passivated Ni/HY and Ni/H-ZSM-5 catalysts. According to the competition with H_2 adsorption on the metallic Ni phase, it is possible that both catalysts lacked the active sites to adsorb MMA and so resulting in their lower ability for MMA hydrogenation.

Among the four zeolite supports, the Ni/H-Beta-27 catalyst showed the best performance for MMA hydrogenation and provided a high MIB yield. Therefore, the Ni/H-Beta-27 catalyst was selected to further investigate the effect of the reaction time, reaction temperature, and initial P_{H2} on the MMA conversion and MIB yield.

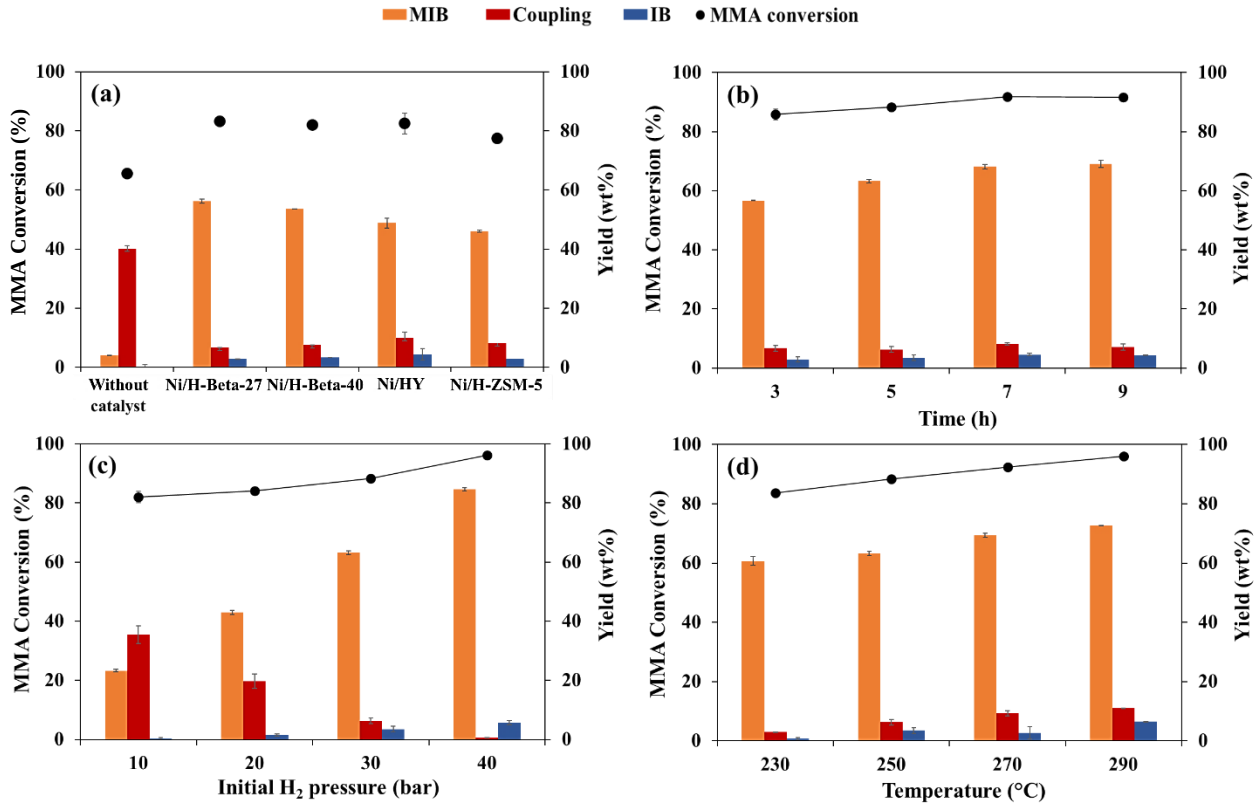

Figure 6 Effects of the (a) zeolite type, (b) reaction time, (c) initial P_{H2}, and (d) reaction temperature on the MMA conversion level and the yields of MIB, IB, and coupling compounds.

Increasing the reaction time from 3 h to 9 h increased the MMA conversion level from 83% to 91% and the MIB yield from 57% to 69%, whereas the yields of IB and coupling compounds remained relatively unchanged (Figure 6b). This indicated that the Ni/H-Beta-27 catalyst had a high selectivity for converting MMA to MIB. Moreover, the longer reaction time suppressed the solid product formation from 14.4 wt% at 3 h to 2.82 wt% at 9 h, resulting in higher yields of both liquid and gaseous products from 80.6 to 88.9 wt% and 5.00 to 8.25 wt%, respectively. Thus, the longer reaction time decreased the level of unsaturated C=C bonds, causing the reduction in the polymerization that forms the solid residue or coke on the catalyst surface (Table 2, Entries 5–8).

From the results shown in Figure 6b, the reaction pathway for MMA hydrogenation over the Ni/H-Beta-27 catalyst under this reaction condition is proposed in Figure 7. Based on the characteristics of the Ni-active metal, the MMA hydrogenation to produce MIB is shown in Route 1. A small portion of MIB could subsequently be transformed to IB via hydrolysis (Route 2) [8]. Since the MMA monomer used as the raw materials for this study contained only 0.67 wt% moisture (measured by Karl Fischer titration technique), the obtained liquid product had an IB portion of less than 5 wt%.

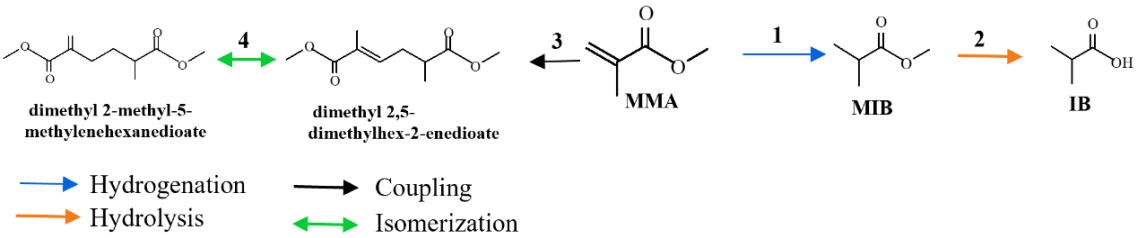

Figure 7 Schematic diagram of MMA hydrogenation over Ni/H-Beta-27 catalyst.

To consider the influence of the initial P_{H2} on the yields and compositions of the liquid products obtained from MMA hydrogenation, the initial P_{H2} was varied over a range of 10–40 bar, keeping the reaction temperature and time constant at 250 °C and 5 h, respectively. The results are summarized in Table 2 (Entries 5 and 9–11) and Figure 6c, and indicated that increasing the initial P_{H2} from 10 to 40 bar resulted in a remarkably higher amount of liquid product from 77.0 to 94.7 wt% with a decreased solid production from 19.2 to 0.54 wt%. Increasing the initial P_{H2} also enhanced the degree of hydrogenation, which led to the greater reduction in unsaturated C=C bonds, decreasing the possibility of polymerization to form a solid residue. In addition, the MMA conversion level was improved from 81.9% to 96.1% when the initial P_{H2} increased from 10 to 40 bar. The increased P_{H2} yielded a higher H_2 concentration around the active sites of the catalyst, and so led to the enhanced degree of hydrogenation. Moreover, the formation of coupling agents was suppressed at a higher initial P_{H2}, presumably due to the saturation of C=C bonds that are the sites for coupling or oligomerization. Together, these resulted in a much higher MIB yield.

The effect of the reaction temperature on MMA hydrogenation was studied over a range of 230–290 °C using the 10 wt% Ni/H-beta-27 catalyst. Increasing the reaction temperature enhanced the liquid and gaseous products from 80.7 to 93.9 wt% and 4.70 to 6.00 wt%, respectively, with a decreasing solid product content from 15.3 to 0.12 wt% (Table 2; Entries 5 and 12–14). Moreover, an increased reaction temperature promoted a higher MMA conversion level from 83.5 to 96.0% and a MIB formation from 60.6 to 72.6 wt% (Figure 6d), but gave a higher amount of coupling compound. Presumably, the high reaction temperature promoted the oligomerization [36], inducing a higher level of liquid products. Thus, a high initial P_{H2} and reaction temperature resulted in a higher MMA conversion level (> 95%) with a high preference to form MIB and suppress solid residue formation.

3.3 Reusability of the catalyst

In this section, the spent Ni/H-Beta-27 catalyst obtained from the MMA hydrogenation at 250 °C under a 30 bar initial P_{H2} for 5 h was used to investigate the catalyst recyclability. After washing with acetone, the spent catalyst was dried at 110 °C for 12 h before recycling under the same reaction conditions for three further consecutive cycles. The MMA conversion level and MIB yield showed only a slight decline over the four consecutive MMA hydrogenation cycles (Figure 8), indicating the remarkable stability of the Ni/H-Beta-27 catalyst.

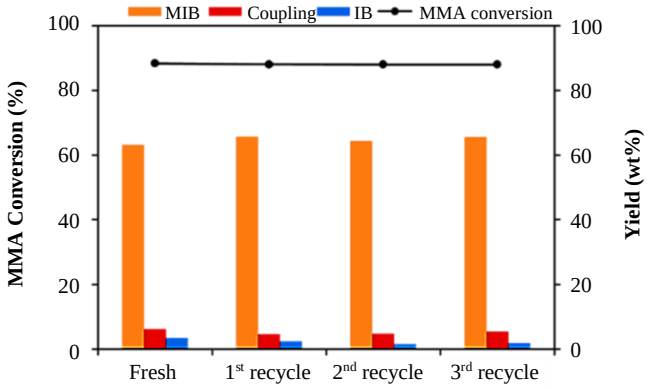

Figure 8 Ability to recycle the Ni/H-beta-27 catalyst, in terms of the obtained MMA conversion level and product yields, for MMA hydrogenation under 30 bar initial P_{H2} at 250 °C for 5 h.

3.4 Hydrogenation of PL-WPMMA

The suitable catalyst and reaction condition obtained from the MMA hydrogenation as described above were then applied to hydrogenate the MMA fraction in the PL-WPMMA. The GC-MS chromatogram of PL-WPMMA (Figure 9a) indicated that MMA was the dominant product with small amounts of some species, such as dimethyl 1,2- cyclopentanedicarboxylate and dimethyl 2,2-bis(2-methyl-2-propenyl)malonate, also being observed. After hydrogenation under 30 bar initial P_{H2} at 250 °C for 5 h, the cyclic compound, 2,3-O-isopropylidene-5[(2-methoxycarbonyl)propyl]), was detected in the liquid product (Figure 9b). This might have resulted from the trace amounts of oligomerized and cyclic compounds present in the PL-WPMMA.

Table 3 shows a comparison of the MMA conversion level and product yields and compositions in the liquid product obtained from the hydrogenation of (i) analytical grade MMA and (ii) PL-WPMMA under 30 bar initial P_{H2} at 250 °C for 5 h. In the case of PL-WPMMA, the MMA conversion level was 99.7%, which was higher than that for the hydrogenation of analytical grade MMA (88.4%). This could be attributed to the presence of 4-methoxyphenol (mequinol) in the analytical grade MMA that is used as an inhibitor of MMA polymerization. Since 4-methoxyphenol could be hydrogenated over the Ni-based catalyst [37], it was possible that 4-methoxyphenol competed with MMA to access the active sites of the catalyst. However, the MIB portion in the hydrogenated PL-WPMMA was only 36.3 wt%, which could be attributed to the presence of oxygen-containing compounds [dimethyl 1,2-cyclopentanedicarboxylate and dimethyl 2,2-bis(2-methyl-2-propenyl)malonate] in the PL-WPMMA. This is because these compounds are precursors to form solid residues that could cover the Ni metal sites [38], allowing the acidic sites of the zeolite support to become dominant. As a result, oligomerization and cyclization reactions over the acidic sites [39] are favored, leading to the higher yield of coupling and cyclic compounds (42.2 wt% and 18.1 wt%, respectively) instead of MIB. These coupling and cyclic compounds also have the potential to transform into the solid residues [40]. In terms of the product yields obtained from the hydrogenation of PL-WPMMA and analytical grade MMA at the same reaction condition, the hydrogenation of PL-WPMMA provided 78.2 wt% liquid product, which was slightly lower than that from the analytical grade MMA (84.7 wt% liquid product). This might be related to the presence of oxygenated compounds in the PL-WPMMA having the potential to form solid residue precursors, as mentioned above, and is in line with the higher solid product obtained from the hydrogenation of PL-WPMMA (16.9 wt%) than that from analytical grade MMA (10.6 wt%).

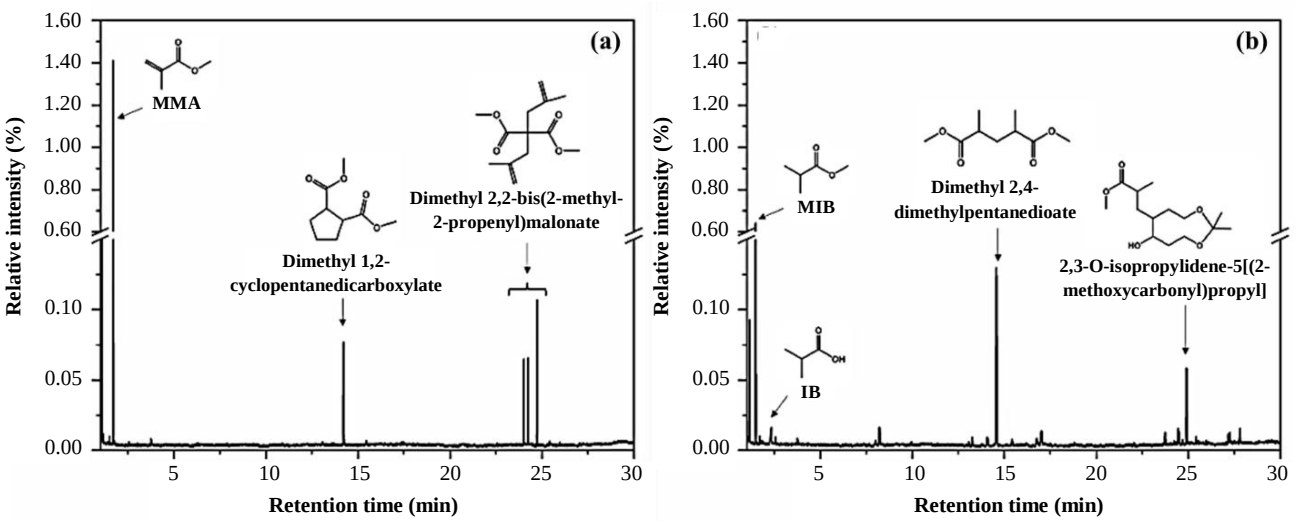

Figure 9 Representative GC-MS chromatograms of PL-WPMMA (a) before and (b) after hydrogenation over the Ni/H-Beta-27 catalyst under 30 bar initial P_{H2} at 250 °C for 5 h.

Table 3 Comparison between the MMA hydrogenation level and obtained products from the hydrogenation of PL-WPMMA and analytical grade MMA

Sample	Initial P_{H2} (bar)	MMA conversion (%)	Product yield (wt%)			Composition in hydrogenated liquid product (wt%)			
			Liquid	Solid	Gas	MIB	IB	Coupling	Cyclics
MMA	30	88.4	84.7	10.6	4.74	63.3	3.53	6.31	0
PL-WPMMA	30	99.7	78.2	16.9	4.93	36.3	3.35	42.2	18.1
	40	100.0	85.8	7.51	6.71	47.6	4.85	37.4	10.4

*PL-WPMMA contained 78 wt% MMA portion.

That the formation of coupling compounds was effectively diminished at the higher initial P_{H2} (Figure 6c) suggests that the initial P_{H2} was the key parameter to control the amount of coupling compounds formed during hydrogenation. When hydrogenation of PL-WPMMA was conducted under 40 bar initial P_{H2} rather than 30 bar, the formation of coupling and cyclic compounds formation was decreased from 42.2 to 37.4 wt% and from 18.1 to 10.4 wt%, respectively, while the MIB yield was improved from 36.3 to 47.6 wt%. Moreover, the liquid product was increased from 78.2 to 85.8 wt% with a reduced solid residue production from 16.9 to 7.51 wt%. This indicated that the higher initial P_{H2} effectively suppressed the coupling and cyclization processes that generated the solid residue precursors.

4. Conclusions

In summary, the H-Beta-27 zeolite was the most efficient support for a Ni-based catalyst (10 wt% Ni/H-Beta-27) for MMA hydrogenation. Based on the obtained results, the Ni/H-Beta-27 catalyst had a high performance for MMA hydrogenation. This was due to its higher external surface area with a larger pore size and the synergistic effect of the Ni-NiO phases in the Ni/H-Beta-27 catalyst. Under 30 bar initial P_{H2} at 250 °C for 5 h, the hydrogenation of analytical grade MMA provided 84.7 wt% liquid products containing 63.2 wt% MIB. Raising the initial P_{H2} to 40 bar increased the MIB yield to 84.6 wt%. In the case of hydrogenation of PL-WPMMA without any purification, hydrogenation of the MMA fraction in the PL-WPMMA under the same condition as stated above gave a 99.7% MMA conversion level, but with only a 36.3 wt% MIB yield. This was attributed to the formation of the oxygenated coupling and cycling compounds at 42 wt% and 18 wt%, respectively. However, the increase in the initial P_{H2} to 40 bar effectively suppressed the production of coupling and cyclic compounds in the hydrogenated PL-WPMMA, and so resulted in a reduced level of solid residue formation. The Ni/H-Beta-27 catalyst had a high stability over at least four consecutive reaction cycles maintaining the same MMA hydrogenation and MIB yield. Hence, the low-cost Ni/H-Beta-27 catalyst could be considered as an effective hydrogenation catalyst for converting MMA to MIB.

5. Acknowledgements

The authors gratefully acknowledge the financial support from Chulalongkorn University. The financial support obtained from Asian & Non-Asian Scholarship for doing the research at Chulalongkorn University is also acknowledged.

6. References

[1] Esmizadeh E, Khalili S, Vahidifar A, Naderi G, Dubois C. Waste polymethyl methacrylate (PMMA): recycling and high-yield monomer recovery. In: Martínez L, Kharissova O, Kharisov B, editors. Handbook of Ecomaterials. Cham: Springer; 2018. p. 1-33.

[2] Moens EKC, De Smit K, Marien YW, Trigilio AD, Van Steenberge PHM, Van Geem KM, et al. Progress in reaction mechanisms and reactor technologies for thermochemical recycling of poly(methyl methacrylate). Polymers. 2020;12(8):1667.

[3] Kaminsky W, Eger C. Pyrolysis of filled PMMA for monomer recovery. J Anal Appl Pyrolysis. 2001;58-59:781-7.
[4] Vassilev I, Hernandez PA, Batlle-Vilanova P, Freguia S, Krömer JO, Keller J, et al. Microbial electrosynthesis of isobutyric, butyric, caproic acids, and corresponding alcohols from carbon dioxide. ACS Sustainable Chem Eng. 2018;6(7):8485-93.
[5] Kelsey DR, Scardino BM, Grebowicz JS, Chuah HH. High impact, amorphous terephthalate copolyesters of rigid 2,2,4,4-tetramethyl-1,3-cyclobutanediol with flexible diols. Macromolecules. 2000;33(16):5810-8.
[6] Zhang K, Woodruff AP, Xiong M, Zhou J, Dhande YK. A synthetic metabolic pathway for production of the platform chemical isobutyric acid. ChemSusChem. 2011;4(8):1068-70.
[7] Besecke S, Schroeder G, Siegert HJ, Gaenzler W, inventors. Method for making isobutyric acid. United State: US Patents 4,452,999. 1987.
[8] Zhou H, Huang Y, Cheng Y, Wang L, Li X. Hydrogenation of methyl methacrylate under mild conditions using biosynthesis Ru catalyst. J Ind Eng Chem. 2017;47:221-7.
[9] Aldea R, Alper H. Ruthenium clay catalyzed chemoselective hydrogenation of unsaturated esters, epoxides, sulfones and phosphonates. J Organomet Chem. 1998;551(1-2):349-54.
[10] Kim YW, Kim MJ. Magnetically recoverable palladium nanocatalyst for chemoselective olefin hydrogenation. Bull Korean Chem Soc. 2010;31(5):1368-70.
[11] Natour S, Abu-Reziq R. Immobilization of palladium catalyst on magnetically separable polyurea nanosupport. RSC Adv. 2014;4:48299-309.
[12] Shesterkina AA, Vikanova KV, Zhuravleva VS, Kustov AL, Davshan NA, Mishin IV, et al. A novel catalyst based on nickel phyllosilicate for the selective hydrogenation of unsaturated compounds. Molec Catal. 2023;547:113341.
[13] André RF, Meyniel L, Carenco S. Nickel carbide (Ni_3C) nanoparticles for catalytic hydrogenation of model compounds in solvent. Catal Sci Technol. 2022;12:4572-83.
[14] Kim J, Han SW, Kim JC, Ryoo R. Supporting nickel to replace platinum on zeolite nanosponges for catalytic hydroisomerization of n-dodecane. ACS Catal. 2018;8(11):10545-54.
[15] Zhuravleva VS, Shesterkina AA, Strekalova AA, Kapustin GI, Dunaev SF, Kustov AL. Microwave synthesis of nickel-based catalysts for selective hydrogenation of phenlacetylene to styrene. Russ J Phys Chem A. 2023;97(10):2120-4.
[16] Phumpradit S, Reubroycharoen P, Kuchonthara P, Ngamcharussrivichai C, Hinchiranan N. Partial hydrogenation of palm oil-derived biodiesel over Ni/electrospun silica fiber catalysts. Catalysts. 2020;10(9):993.
[17] Cuevas-García R, Téllez-Romero JG, Ramírez J, Sarabia-Bañuelos P, Puente-Lee I, Salcedo-Luna C, et al. Effect of the preparation method on particle size and reaction selectivity on naphthalene hydrogenation over Ni/H-MOR catalysts. Catal Today. 2021;360:63-71.
[18] Song W, Liu Y, Baráth E, Zhao C, Lercher JA. Synergistic effects of Ni and acid sites for hydrogenation and C–O bond cleavage of substituted phenols. Green Chem. 2015;17:1204-18.
[19] Luo CW, Li A. Synthesis of 3-picoline from acrolein dimethyl acetal and ammonia over NH4F-HF treated ZSM-5. Reac Kinet Mech Cat. 2018;125(1):365-80.
[20] Bhavani AG, Kim WY, Kim JY, Lee JS. Improved activity and coke resistance by promoters of nanosized trimetallic catalysts for autothermal carbon dioxide reforming of methane. Appl Catal A-Gen. 2013;450:63-72.
[21] Gong H, Xiao Z, Zhuang Y, Liang S, Li X, Zheng W. Core-shell meso-beta@mesoporous aluminosilicate supported Ni_2P catalyst for the hydrodenitrogenation of quinoline: effect of core shell structure on Ni_2P particle size. Fuel. 2021;302:121131.
[22] Chintakanan P, Vitidsant T, Reubroycharoen P, Kuchonthara P, Kida T, Hinchiranan N. Bio-jet fuel range in biofuels derived from hydroconversion of palm olein over Ni/zeolite catalysts and freezing point of biofuels/Jet A-1 blends. Fuel. 2021;293:120472.
[23] Lima PM, Garetto T, Cavalcante CL, Cardoso D. Isomerization of n-hexane on Pt–Ni catalysts supported on nanocrystalline H-BEA zeolite. Catal Today. 2011;172(1):195-202.
[24] Liu Q, Zuo H, Wang T, Ma L, Zhang Q. One-step hydrodeoxygenation of palm oil to isomerized hydrocarbon fuels over Ni supported on nano-sized SAPO-11 catalysts. Appl Catal A-Gen. 2013;468:68-74.
[25] Tieuli S, Mäki-Arvela P, Peurla M, Eränen K, Wärnå J, Cruciani G, et al. Hydrodeoxygenation of isoeugenol over Ni-SBA-15: Kinetics and modelling. Appl Catal A-Gen. 2019;580:1-10.
[26] Penkova A, Dzwigaj S, Kefirov R, Hadjiivanov K, Che M. Effect of the preparation method on the state of nickel ions in BEA zeolites. A study by Fourier transform infrared spectroscopy of adsorbed CO and NO, temperature-programmed reduction, and X-Ray diffraction. J Phys Chem C. 2007;111(24):8623-31.
[27] Sahle-Demessie E, Devulapelli VG, Hassan AA. Hydrogenation of anthracene in supercritical carbon dioxide solvent using Ni supported on Hβ-zeolite catalyst. Catalysts. 2012;2(1):85-100.
[28] Peron DV, Zholobenko VL, de la Rocha MR, de Souza MD, Feris LA, Marcilio NR, et al. Nickel–zeolite composite catalysts with metal nanoparticles selectively encapsulated in the zeolite micropores. J Mater Sci. 2019;54(7):5399-411.
[29] Yang H, Han T, Yang W, Sandström L, Jönsson PG. Influence of the porosity and acidic properties of aluminosilicate catalysts on coke formation during the catalytic pyrolysis of lignin. J Anal Appl Pyrolysis. 2022;165:105536.
[30] Huang J, Jiang Y, Reddy Marthala VR, Bressel A, Frey J, Hunger M. Effect of pore size and acidity on the coke formation during ethylbenzene conversion on zeolite catalysts. J Catal. 2009;263(2):277-83.
[31] Chen S, Qian TT, Ling LL, Zhang W, Gong BB, Jiang H. Hydrogenation of furfural to cyclopentanone under mild conditions by a structure-optimized $Ni{-}NiO/TiO_2$ heterojunction catalyst. ChemSusChem. 2020;13(20):5507-15.
[32] Song S, Yao S, Cao J, Di L, Wu G, Guan N, et al. Heterostructured Ni/NiO composite as a robust catalyst for the hydrogenation of levulinic acid to γ-valerolactone. Appl Catal B-Environ. 2017;217:115-24.
[33] Motahari F, Mozdianfard MR, Salavati-Niasari M. Synthesis and adsorption studies of NiO nanoparticles in the presence of H_2acacen ligand, for removing Rhodamine B in wastewater treatment. Process Saf Environ Prot. 2015;93:282-92.
[34] Yaocíhuatl MG, Martín HL, Jorge AC. Dimerization of isobutene over nickel modified zeolites to obtain isooctene. Catal Lett. 2006;110(1):107-13.
[35] Oehme G, Grassert I, Mennenga H, Baudisch H. On the mechanism of the Pd(II)-catalyzed dimerization and codimerization of methyl methacrylate: application of deuterium exchange experiments. J Mol Catal. 1986;37(1):53-62.
[36] Chanyshev AD, Litasov KD, Furukawa Y, Kokh KA, Shatskiy AF. Temperature-induced oligomerization of polycyclic aromatic hydrocarbons at ambient and high pressures. Sci Rep. 2017;7(1):7889.

[37] She T, Chu X, Zhang H. Dong J, Niu L, Lan X, et al. Ni-Mg/γ-Al_2O_3 catalyst for 4-methoxyphenol hydrogenation: effect of Mg modification for improving stability. J Nanopart Res. 2018;20:224.
[38] Hu X, Zhang Z, Gholizadeh M, Zhang S, Lam CH, Xiong Z, et al. Coke formation during thermal treatment of bio-oil. Energy Fuels. 2020;34(7):7863-914.
[39] Koninckx E, Mendes PSF, Thybaut JW, Broadbelt LJ. Ethylene oligomerization on nickel catalysts on a solid acid support: from New mechanistic insights to tunable bifunctionality. Appl Catal A-Gen. 2021;624:118296.
[40] Anand M, Farooqui SA, Kumar R, Joshi R, Kumar R, Sibi MG, et al. Optimizing renewable oil hydrocracking conditions for aviation bio-kerosene production. Fuel Process Technol. 2016;151:50-8.